International Journal of Hybrid Information Technology
Vol.7, No.3 (2014), pp.65-84
http://dx.doi.org/10.14257/ijhit.2014.7.3.09

Improved Bias-corrected Fuzzy C-means Segmentation of Brain MRI Data

Ahmed Al-Taie[1, 3], Horst K. Hahn[1, 2], and Lars Linsen[1]

[1]*Jacobs University, Bremen, Germany*
[2]*Fraunhofer MEVIS, Bremen, Germany*
[3]*Computer Science Department, College of Science for women, Baghdad University, Baghdad, Iraq*

{a.altaie, h.hahn, l.linsen}@jacobs-university.de, horst.hahn@mevis.fraunhofer.de

Abstract

Errors in the scanning procedures lead to uncertainties when trying to segment the scanned images. Fuzzy c-means is a clustering method that can be applied to segment images with uncertainty estimates. Bias-corrected fuzzy c-means (BCFCM) clustering compensates for two sources of uncertainty by modeling noise and bias fields during the segmentation process. In this paper, we present an approach to improve BCFCM clustering and apply it to magnetic resonance imaging (MRI) data of the human brain. Our approach is based on two variants of BCFCM clustering, the classical one and the one with distance-based weights. We improve both variants by slightly modifying their main algorithms for better bias field estimation. To evaluate the improved algorithms, we apply the algorithms to synthetic data, simulated MRI brain data, and real MRI brain data with ground truth in form of manual segmentation. All experiment results show that our improved methods outperform the original methods in both the segmentation accuracy and efficiency (the number of iterations).

Keywords*: Image segmentation, Fuzzy c-means, Modified fuzzy c-means, Brain MRI segmentation, Bias field*

1. Introduction

Image segmentation plays a vital role in a broad range of computer vision and image processing applications such as object or pattern recognition, geographical imaging, geology, remote sensing, and medical imaging. In image segmentation, images are partitioned into disjoint regions of homogeneous properties. For segmenting human brain images in a biomedical context, the regions of interest are the tissues of white matter (WM), gray matter (GM), and cerebrospinal fluid (CSF). Several studies show that physiological processes and disease severity can be characterized based on the composition changes of these tissues in the whole volume or within specific regions [1, 2]. Magnetic resonance imaging (MRI) is one of the most commonly used medical imaging techniques due to its ability to distinguish soft tissues and because it does not rely on x-ray technology. In human brain image segmentation of MRI data, the task is to specify the tissue type for each pixel (when operating on a 2D slice) or voxel (when operating on the 3D volume data), on the basis of the measured MRI values and prior knowledge about the brain. This segmentation step is crucial for many medical analyses and clinical applications, such as the visualization and analysis of anatomical structures, detection of pathology, and surgical planning. It is also an important step for further processing tasks such as visualization, multimodal data fusion and

ISSN: 1738-9968 IJHIT

registration, and surgical navigation. However, brain segmentation is also a complex and challenging task due to overlapping ranges of intensity values of tissue types and the imaging artifacts such as noise, intensity in-homogeneity, and partial volume effect. Fuzzy c-means is one of the most used algorithms for image segmentation [3-10]. Its main advantages include a straightforward implementation, the applicability to multichannel data, its robustness in the absence of prior knowledge about cluster centers, robustness when the number of classes is known as in our problem of human brain segmentation, and the ability to model uncertainty within the data.

The main focus of this paper is to improve the result of certain segmentation outputs by reducing the effect of some uncertainty sources on the results. We base our work on the approaches of bias-corrected fuzzy c-means (BCFCM) clustering [9] and its variant with distance-based weights [10], see Section 3. We chose those fuzzy c-means implementations as they compensate for two sources of uncertainty, noise and bias fields.

We improve the performance of the two segmentation methods by slightly modifying their algorithms, see Section 4. The experimental results show that our improved methods outperform the original methods in both the segmentation accuracy and efficiency (number of iterations) for all our examples. We compare our method to the original works when applied to synthetic data, simulated MRI brain data, and real MRI brain data, where the ground truth is given by manual segmentations of medical experts, see Section 5.

2. Related Work

Recently, in medical imaging many researchers have tried to modify the original fuzzy c-means (FCM) algorithm [3-10], in order to improve the final segmentation results, and consequently to reduce the amount of uncertainty in the respective results. Pham [4] generalized the FCM objective function by including a spatial penalty term on the membership function to be more robust to noise and other imaging artifacts when compared to the standard algorithm. Chuang *et al.* [7] follow up [4] in utilizing the spatial information in the image for further improve the segmentation performance. They use a special spatial function in the weighted summation of membership function of the neighborhood voxels to adjust the membership value of the center voxel. This leads to more homogeneous region and removes noisy spots.

Zhang and Chen [6] replaced the Euclidean distance in the FCM algorithm with a kernel-induced distance to construct a non-linear version of the linear algorithm. Furthermore, they added a spatial penalty term to act as regularizer. Mohammed *et al.* [3] use a modified version of the Euclidean-distance approach that involves the membership value and the spatial distance of the neighbor voxels to make the method less sensitive to noise while enhancing the edges. Szilágyi *et al.* [11] introduced the enhanced fuzzy c-means algorithm (EnFCM) that modifies the FCM algorithm such that the objective function is based on the number of intensity levels available in the image but not on the number of voxels. This modification led to a very fast algorithm that slightly improves the segmentation result. Ahmed *et al.* [9] proposed an algorithm to compensate inhomogeneity and to label a pixel considering its immediate neighborhood. This algorithm is called bias-corrected fuzzy c-means (BCFCM). The BCFCM method is a common reference for most of the modified fuzzy c-means algorithms that were introduced later and its objective function is used as basis for their modifications. Yuan *et al.* [10] enhanced the method by replacing the fixed value of the alpha parameter that controls the influence of the neighborhood voxels during optimization with a weighted function that varies according to the closeness of the intensity of each neighboring

voxel to the center voxel (voxel under consideration). We refer to this algorithm as bias-corrected fuzzy c-means with weighted alpha (BCFCM_WA).

Li *et al.* proposed a new energy minimization method based on coherent local intensity clustering (CLIC) for simultaneous tissue classification and bias field estimation of MR images [12]. For each pixel, a clustering criterion function is defined with the clustering centers replaced by the product of the bias within a neighborhood and the clustering centers. In addition, a weight for each pixel is introduced to control its influence on the clustering criterion function. A pixel at location far from the neighborhood center should have less influence on the clustering criterion function than the closer pixels. Integration of the clustering criterion function leads to an energy, whose minimization leads to simultaneous tissue classification and bias field estimation. The CLIC algorithm is sensitive to the choice of the parameter of the weighting function. In addition, the spatially coherent nature of the CLIC criterion function that omits the local gray level relationship makes the estimated membership functions inaccurate, and finally causes misclassifications, especially for the pixels around the boundaries. In order to reduce the noise effect during segmentation, Wang *et al.* [13] introduced a method that incorporates both the local spatial context and the non-local information into the standard FCM algorithm using a dissimilarity index instead of the usual distance metric. Ji *et al.* [14] follow up on Wang et al.'s approach by using the local spatial context and non-local information to develop the possibilistic fuzzy c-means clustering algorithm PFCM. Unfortunately, the two methods by Wang *et al.* and Ji *et al.* are computationally expensive which made them impractical.

We improve the performance of the BCFCM and BCFCM_WA segmentation methods by slightly modifying their algorithms. We decided to choose these two algorithms because of their ability to compensate for two important sources of uncertainty in their segmentation model. First, they compensate for noise in the image by involving neighbor voxels and intensity in-homogeneity by estimating bias field. However, these algorithms still have limitations. Through deep analysis to these algorithms, we discovered two of these limitations.

In this paper, we propose an appropriate modification to increase the performance. These modifications are using lower base for log transform to reduce the negative effect of this transform on data classification and slowing the updating of the bias field estimation to avoid over-estimation. The experimental results show that our improved methods outperform the original methods.

3. FCM Methods

In this section, we describe the standard FCM and the bias-corrected segmentation approaches BCFCM by Ahmed *et al.* [9] and BCFCM WA by Yuan *et al.* [10]. Our approach is an improvement of their techniques, which will be detailed in the subsequent section.

3.1. Standard FCM Approach

The standard fuzzy c-means (FCM) approach is an iterative, unsupervised algorithm initially introduced by Bezdek [15]. The FCM objective function for partitioning an image with N pixels or voxels $\{x_k\}_{k=1}^{N}$ into c clusters is given by

$J_{FCM} = \sum_{i=1}^{c} \sum_{k=1}^{N} u_{ik}^{p} \left\| x_k - v_i \right\|^2$, where $\{v_i\}_{i=1}^{c}$ are the representatives of the clusters and the matrix $[u_{ik}] = U$ represents a partition matrix of size $c \times N$ with $U \in \mathcal{U}$ according to

$$\upsilon = \{u_{ik} \in [0,1] \mid \sum_{i=1}^{c} u_{ik} = 1 \ \forall k \ \wedge \ 0 < \sum_{k=1}^{N} u_{ik} \leq N \ \forall i\}.$$

The entries u_{ik} can be interpreted as the probability that pixel x_k belongs to cluster *i*. This is referred to as fuzzy membership. The parameter *p* is a weighting exponent on each fuzzy membership and determines the amount of fuzziness of the resulting classification. The algorithm is initialized with some representatives v_i for each cluster and the memberships are updated to minimize the objective function J_{FCM}.

3.2. BCFCM Approach

Ahmed *et al.* [9] proposed to model an MRI signal as the true signal intensity *X* generated by the underlying anatomy multiplied by a spatially varying factor called the gain field *G* leading to pixel values

$$Y_k = X_k G_k \forall k \in \{1,2,..., N\} \qquad (1)$$

i.e., groups X_k, Y_k, and G_k are the true intensity, observed intensity, and the gain field at the k_{th} pixel, respectively, *N* is, again, the total number of pixels in the MRI data set. The artifact can be modeled as an additive bias field by applying a logarithmic transformation to (1) leading to

$$y_k = x_k + \beta_k \forall k \in \{1,2,..., N\},$$

where x_k and y_k are the true and observed log-transformed intensities at the k_{th} pixel, respectively, and β_k is the bias field at the k_{th} pixel. If the bias field model is incorporated into a FCM segmentation, it is easy to estimate the tissue class by applying the segmentation to the corrected data. Ahmed *et al.* [9] modified the objective function of the standard fuzzy c-means (FCM) algorithm to compensate for intensity inhomogeneities and to allow the labeling of a pixel (voxel) to be influenced by the labels in its immediate neighborhood. Using the notations from above, the objective function can be written as

$$J_m = \sum_{i=1}^{c} \sum_{k=1}^{N} u_{ik}^{p} \left\| y_k - \beta_k - v_i \right\|^2 + \frac{\alpha}{N_r} \sum_{i=1}^{c} \sum_{k=1}^{N} u_{ik}^{p} \gamma_i,$$

where N_k is the set of neighboring pixels of pixel y_k, N_r is the number of considered neighbors, $\gamma_i = \sum_{y_r \in N_k}^{c} \left\| y_k - \beta_r - v_i \right\|^2$, and α is a constant that regulates how much neighborhood information influences the result. The neighborhood term acts as a regularizer and biases the solution towards piecewise-homogeneous labeling. The objective function of BCFCM is minimized by taking the first derivatives of J_m with respect to u_{ik}, v_i, β_k, and setting them to zero. This results in three necessary but not sufficient conditions for J_m to be at a local minimum.

- Membership Evaluation

$$u_{ik}^{*} = \frac{1}{\sum_{j=1}^{c} \left(\frac{D_{ik} + (\alpha / N_R)\gamma_i}{D_{jk} + (\alpha / N_R)\gamma_j} \right)^{\frac{1}{p-1}}}, \qquad (2)$$

  Where $D_{ik} = \left\| y_k - \beta_r - v_i \right\|^2$.

- Cluster Prototype Updating

$$v_i^{*} = \frac{\sum_{k=1}^{N} u_{ik}^{p} \left((y_k - \beta_k) + (\alpha / N_R) \sum_{y_r \in N_k} (y_r - \beta_r) \right)}{(1+\alpha) \sum_{k=1}^{N} u_{ik}^{p}} \qquad (3)$$

- Bias-Field Estimation

$$\beta_k^* = y_k - \frac{\sum_{i=1}^{c} u_{ik}^p v_i}{\sum_{i=1}^{c} u_{ik}^p} \quad (4)$$

3.3. BCFCM_WA Approach

Yuan *et al.* [10] modify the objective function of BCFCM algorithm by replacing the fixed weight (α / N_R) that controls the participation of neighborhood voxels in updating the membership values of the considered voxel with a variable weight for each neighbor voxel. This leads to the updated objective function

$$J_y = \sum_{i=1}^{c}\sum_{k=1}^{N} u_{ik}^p D_{ik} + \sum_{i=1}^{c}\sum_{k=1}^{N} u_{ik}^p \sum_{y_r \in N_k} \omega(y_k, y_r) D_{ir},$$

where $\omega(y_k, y_r)$ is a weighting function (e.g. $\omega(y_k, y_r) = \alpha e^{\left(\|y_k - y_r\|^2 / \sigma^2\right)}$), satisfies the conditions $\sum_{y_r \in N_k} \omega(y_k, y_r) = \alpha$, $0 < \alpha < 1$, $\forall k \in \{1,2,..., N\}$, and $D_{ir} = \left\|y_r - \beta_r - v_i\right\|^2$.

When choosing $\omega(y_k, y_r) = (\alpha / N_R)$, the objective function J_y is BCFCM objective function proposed by Ahmed *et al.* [9]. The three necessary but not sufficient conditions for J_y to be at a local minimum are given by

- Membership Evaluation

$$u_{ik}^* = \frac{1}{\sum_{j=1}^{c} \left(\frac{D_{ik} + \gamma_i}{D_{jk} + \gamma_j} \right)^{\frac{1}{p-1}}}, \quad (5)$$

  where $D_{ik} = \left\|y_k - \beta_k - v_i\right\|^2$, and $\gamma_i = \sum_{y_r \in N_k}^{c} \omega(y_k, y_r) \left\|y_k - \beta_r - v_i\right\|^2$.

- Cluster Prototype Updating

$$v_i^* = \frac{\sum_{k=1}^{N} u_{ik}^p \left((y_k - \beta_k) + \sum_{y_r \in N_k} \omega_{kr} (y_r - \beta_r) \right)}{\sum_{k=1}^{N} u_{ik}^p \left(1 + \sum_{y_r \in N_k} \omega_{kr} \right)}, \quad (6)$$

  where ω_{kr} is equal to $\omega(y_k, y_r)$.

- Bias-Field Estimation

$$\beta_k^* = y_k - \frac{\sum_{i=1}^{c} v_i \left(u_{ik}^p + \sum_{y_r \in N_k} \omega_{kr} u_{ir}^p \right)}{\sum_{i=1}^{c} \left(u_{ik}^p + \sum_{y_r \in N_k} \omega_{kr} u_{ir}^p \right)}. \quad (7)$$

3.4. Optimization Algorithm

The BCFCM and BCFCM_WA algorithms for correcting the bias field and segmenting the image into different clusters can be summarized by the following steps:

1. Choose the initial representatives $\{v_i\}_{i=1}^{c}$. Initialize $\{\beta_k\}_{k=1}^{N}$ with very small and equal values (*e.g.*, 0.01).
2. Update the partition matrix using (2) for BCFCM method and (5) for BCFCM_WA method.
3. Re-compute the representatives of the clusters in the form of weighted averages of the patterns using (3) for BCFCM method and (6) for BCFCM_WA method.
4. Estimate the bias term using (4) for BCFCM method and (7) for BCFCM_WA method.

Repeat steps (2−4) until the termination criterion

$$\left\| V_{new} - V_{old} \right\| < \varepsilon$$

is met, where $\|.\|$ is the Euclidean norm, V_{old} and V_{new} are the vectors of cluster representatives before and after the most recent step, and ε is a (typically small) user-defined error tolerance.

4. Improved Methods

The main drawbacks of the above two algorithms BCFCM and BCFCM_WA are the log transform and the overestimation of the bias field in some situations which can lead to misclassification. We propose two modifications, which apply to both the BCFCM and the BCFCM_WA algorithm. The modifications are small, but we show in the subsequent section that it can have a big impact.

4.1. Adjusting the log transform

When we apply the log transform on a certain dataset, the range of the transformed data is contracted. This contraction affects the behavior of the clustering algorithm negatively especially when the data are noisy and the discriminatory power of the clustering algorithm is decreased. Because the distance among clusters representatives is smaller in the transformed space and some extreme points in one class become closer to the center of the neighboring class, it may be misclassified. To reduce this negative effect of the log transform, we propose to use a logarithm with a lower base (*e.g.* $log_{1.15}$ or $log_{1.5}$) instead of using the natural logarithm (*i.e.* the logarithm to log base $e \approx 2.719$). This reduce the contraction ratio of the transformed data. To further reduce this contraction effect we also investigated scaling all intensities with a constant before starting the algorithm. In our experiments we found out that this is beneficial for the improved version of the BCFCM_WA method. We apply a scaling with factor 10.

4.2. Avoiding bias field overestimation

The second drawback that we tackled is the over-estimation of the bias field, which can lead to false classification. In order to avoid an overestimation we propose to slow down the estimation of the bias field compared to the estimation of the partition matrix. Hence, in the two algorithms BCFCM and BCFCM_WA we modify the procedure such that the update of the bias field βk is only done once every n iterations (*e.g.* n=4 or n=5). This modification has the nice side effect that less computation is necessary. First, the overall bias-field estimation time is obviously reduced and, second, when not updating the bias field β_k the terms $(y_k-\beta_k)$ and $(y_r-\beta_r)$ do not need to be re-computed.

A general drawback of FCM algorithms is that the update of the cluster representatives (see Equations (3) and (6)) is based on the weighted averages of all pixels, which may lead to the production of "pseudo centroids". Especially for class with small size, the participation of a large number of pixels from outside the class (even though multiplied with small weights) may balance or overcome the effect of participation of a small number of pixels from within

the class (even though multiplied with large weights). To avoid and to compute more accurate cluster representatives, we update the cluster representatives by only using pixels that have a large probability of belong to the respective class, *e.g.*, by having entries U_{ik}>0.5 in the partition matrix. Again, in addition to increasing the clustering result, this modification saves some computations.

5. Results and Discussion

In this section, we present and compare the experimental results when applying the original and the improved methods on synthetic images, simulated MRI brain images [16], and real MRI T1-weighted brain images [17]. The reasons for using digitally simulated images are the prior knowledge of the true tissue types and the control over image parameters such as mean intensity values, noise, and intensity inhomogeneities.

To mimic the main brain tissues of MRI T1 and T2 images in a synthetic image (*i.e.* the background Bg, the white matter WM, The gray matter GM, and the cerebrospinal fluid CSF), we generate an example of four respective classes with complex structures as shown in Figure 1. We believe that our examples mimics the structures in an MRI brain image better than the two-classes synthetic image of [9] or [5] and the four-classes synthetic image of [7]. We corrupted our synthetic image with different types of noise that are common in medical data such as Gaussian, salt-and-pepper, or sinusoidal noise, or a combination of them.

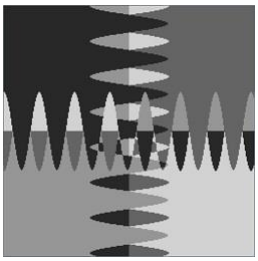

Figure 1. Synthetic Images with Four Classes

As initialization for clusters' representatives in the synthetic example, we use the class centroids of the synthetic image before corrupting it with noise. For the experiments on the simulated and real brain MRI images, we initialize the representatives of clusters based on the segmentation result of the EnFCM algorithm [11] which is very fast and gives acceptable segmentation (to some degree). This choice is suitable for experiments assuming the absence of ground truth and prior knowledge. In order to compare the performance of the proposed methods with the original methods (*i.e.*, the BCFCM [9] and BCFCM_WA [10]), we employed the segmentation accuracy SA measure and Jaccard measure JM to evaluate the differences among them
:

$$SA = \frac{Number\ \ of\ \ correctly\ \ classified\ \ pixels}{Total\ \ number\ \ of\ \ pixels} \times 100\ \ \%$$

$$JM_{\ j} = \frac{A_j \cap A_{refj}}{A_j \cup A_{refj}} \times 100\ \ \%$$

Where A_{refj} represents the set of pixels belonging to the j_{th} class of the reference segmented image and A_j represent the set of pixels belonging to the j_{th} class found by the algorithm.

In our experiments, we use the same parameters that are used by the original methods [9], (*i.e.* α=0.85, *p*=2, ε=0.01), but for the number of pixels in the neighborhood window N_R we use eight instead of nine by excluding the center pixel (*i.e.*, the pixel under consideration). For parameters σ and α of the weight function ω in the BCFCM_WA method [10], we also use the same values as the original paper (*i.e.* σ=1.25 and α=0.09).

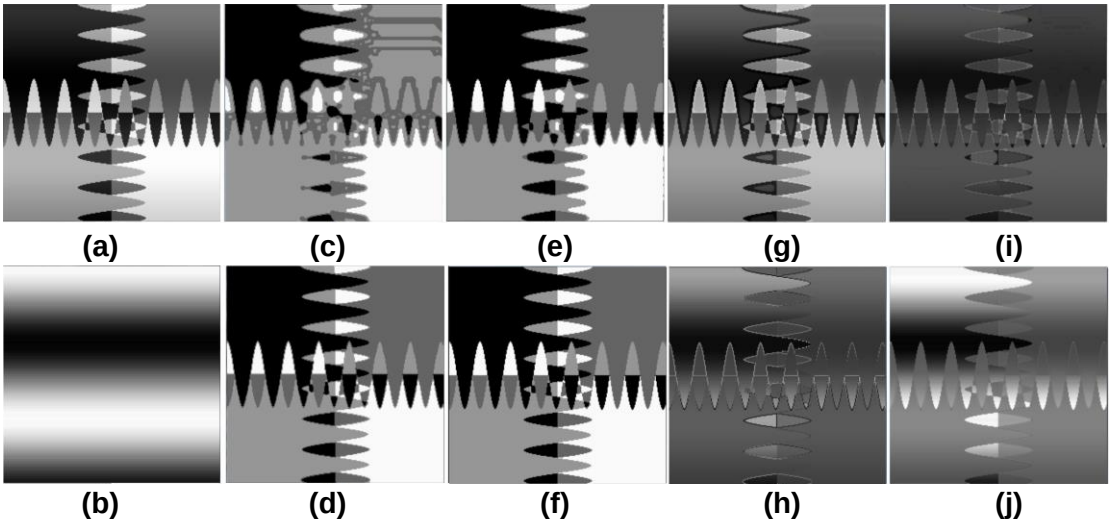

Figure 2: Comparison of segmentation results and bias field estimation on synthetic image with four classes corrupted with sinusoidal noise, (a) original synthetic image corrupted with sinusoidal noise, (b) sinusoidal bias field, (c) BCFCM result, (d) IBCFCM result, (e) BCFCM_WA result, and (f) IBCFCM_WA result, (g) BCFCM bias field, (h) IBCFCM bias field, (i) BCFCM_WA bias field, and (j) IBCFCM_WA bias field.

In the first group of experiments, we applied the four methods on synthetic images with four classes to explore how the proposed modifications improve the results. In the first experiment, we use the synthetic image of Figure 1, corrupted by a sinusoidal noise that models bias field errors. We apply the two original methods BCFCM and BCFCM_WA and our improved versions denoted by IBCFCM and IBCFCM_WA, respectively. From the results shown in Figure 2, we observe how the proposed methods improve the segmentation result and the bias field estimation, respectively. In the second experiment, we use the synthetic image of Figure 1 corrupted by a mixture of Gaussian noise with mean 0 and variance 64, 5% of salt-and-pepper noise, and a sinusoidal noise that models bias field errors. The result of applying the four methods to this image shows how our improvements outperform the original methods, see Figure 3 and Table 1.

The numbers in Table 1 indicate that segmentation accuracy is higher both for IBCFCM when compared to BCFCM and for IBCFCM_WA when compared to BCFCM_WA. Also, the Jaccard measures are generally higher for our improved methods. To show that this is also true for other combinations of noise, we list a few in Table 2. Segmentation accuracy was always highest for IBCFCM_WA and second-highest for IBCFCM. In Figure 3, we can observe clearly how the BCFCM method produces undesired results, which we believe is due to the over-estimation of the bias field for some noisy pixels, *i.e.*, the bias field estimation increased over the number of iterations and eventually led to a misclassification. Our improved methods, on the contrary, prevent the aggregation of small errors in the bias field

estimation by only update the bias field once a good estimation for the clusters' representatives has been found. The BCFCM_WA result shows that the border of segments are deformed while our improved version does not exhibit such artifacts, as the more accurate bias field estimation prevents the smoothing effect of neighborhood's window on the noisy pixels in the partial volume areas. The more accurate estimation of the bias field is made explicit in Figure 4, which shows a comparison of the used noise image and the estimated bias fields for the four methods as in the experiment of Figure 3.

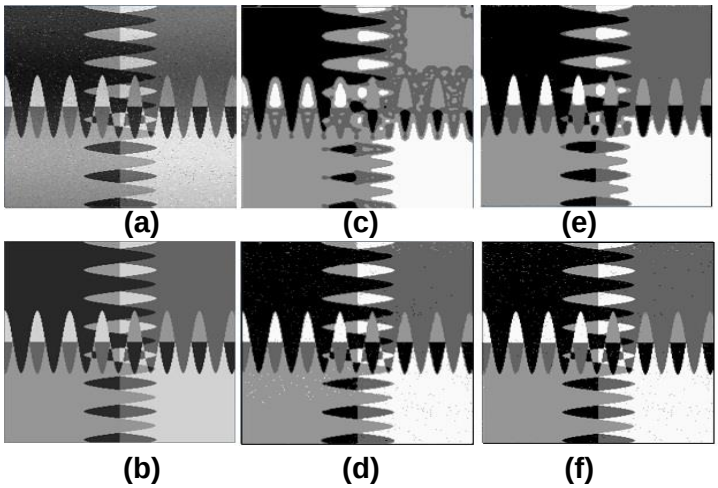

Figure 3: Comparison of Segmentation Results on Synthetic Image Corrupted with Mixed Noise (a), (b) Original Synthetic Image, (c) BCFCM result, (d) IBCFCM result, (e) BCFCM_WA result, and (f) IBCFCM_WA result.

Table 1: Segmentation Accuracy (SA) and Jaccard Measure (JM) in Percentage for the Four Methods on Synthetic Image with Four Classes Corrupted by Mixed Noise.

Figure 3 (a)	SA%	Class1 JM%	Class2 JM%	Class3 JM%	Class4 JM%
BCFCM	85.3317	74.8591	87.6736	73.4618	66.0604
IBCFCM	95.5399	95.8304	92.5754	88.4696	88.6968
BCFCM_WA	94.3192	98.2383	88.2528	83.3352	86.1636
IBCFCM_WA	98.8068	97.8091	98.5026	96.5281	97.8626

Table 2: Segmentation Accuracy (SA) in Percentage for the Four Methods on Synthetic Image Corrupted with Different Combinations of Noise.

Noise Type	BCFCM	IBCFCM	BCFCM_WA	IBCFCM_WA
SaP* 5% & Sin	83.8348	95.4498	94.6625	98.9639
G(0,64) & Sin	77.7756	96.3013	94.8166	99.6353
SaP & G(0,64)	81.4316	96.817	94.1544	99.2599
Sin	76.1353	96.373	94.7708	99.9832
SaP 5%	79.2358	97.2137	94.4046	99.0952
G(0,64)	78.4637	97.4915	94.8761	99.9908

* SaP=Salt-and-Pepper; G=Gaussian; Sin=Sinusoidal

In the second group of experiments, we use the simulated MRI brain images of different modalities (T1-weighted, T2-weighted and PD-weighted) corrupted by different level of

Gaussian noise (3%, 5%, 7%) with and without 20% intensity inhomogeneity. Figures 5, 6, and 7 show a comparison among the segmentation results when applying the four methods on the simulated T1-, T2-, and PD-weighted MRI brain images with 5% Gaussian noise and 20% intensity inhomogeneity, while the Tables 3, and 4 show the comparison of the segmentation accuracies when applying the four methods to the three modalities corrupted with different levels of noise. The outcome is similar to the one before, as our improved algorithms outperform the original one for all the given examples independent of noise level or imaging modality.

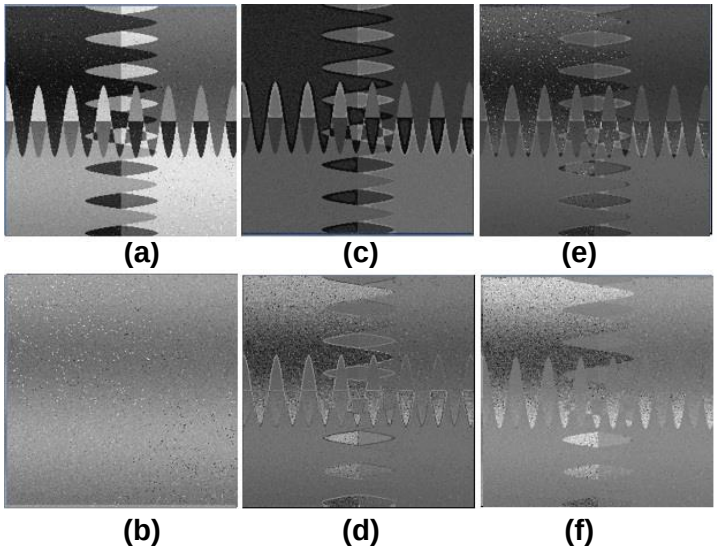

Figure 4. Comparison of Bias Field Estimation in the Experiment of Figure 3. (a) Original Image Corrupted with Mixed Noise, (b) Original Noise Image, (c) Bias Field for BCFCM, (d) Bias Field for IBCFCM, (e) Bias Field for BCFCM_WA, (f) Bias Field for IBCFCM_WA

Furthermore, Figure 8 shows the bias field estimation and image correction comparisons for the four methods on simulated T2-weighted MR image corrupted with 40% intensity inhomogeneity. We can easily observe the improvement of the proposed methods in the bias field estimation in all experiments.

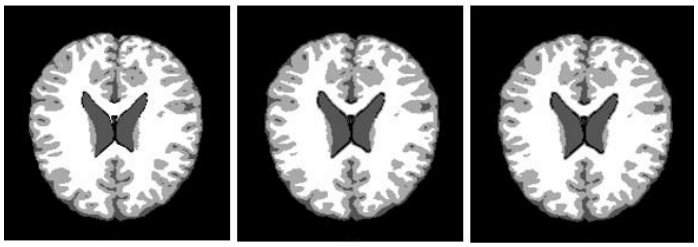

Figure 5: Comparison of segmentation results on simulated T1-weighted MR brain image corrupted with 5% Gaussian noise and 20% intensity inhomogeneity: (a) original image corrupted with noise, (b) ground truth segmentation, (c) BCFCM result, (d) IBCFCM result, (e) BCFCM_WA result, (f) IBCFCM_WA result.

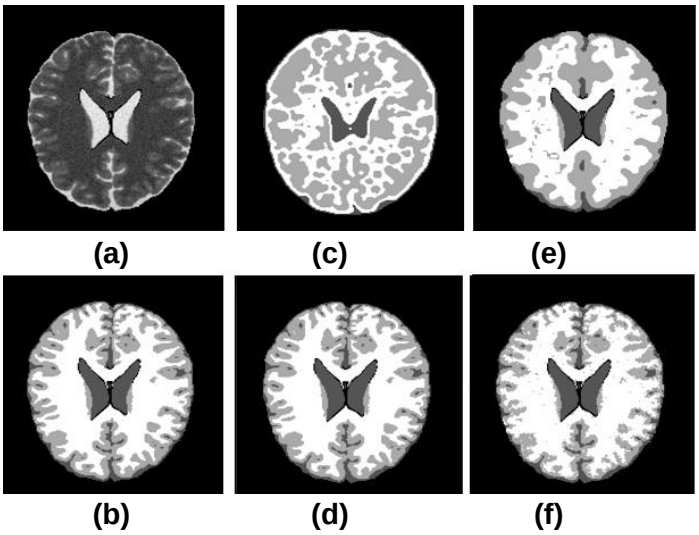

Figure 6: Comparison of segmentation results on simulated T2-weighted MR brain image corrupted with 5% Gaussian noise and 20% intensity inhomogeneity: (a) original image corrupted with noise, (b) ground truth segmentation, (c) BCFCM result, (d) IBCFCM result, (e) BCFCM_WA result, (f) IBCFCM_WA result.

In addition to the synthetic images and simulated MRI brain images, we apply our methods to real T1-weighted MRI images [17]. We evaluate the segmentation accuracy based on the ground truth for these images in form of provided manual segmentation results. Figure 9 shows the comparison among the segmentation results when applying the four methods beside the original fuzzy c-means algorithm (FCM) to two slices. Table 5 shows the comparison among segmentation accuracy results in Figure 9. All experiments show that the improved methods outperform the original methods and that the IBCFCM_WA algorithm is superior over all methods on all experiments.

An important difference between our experiments and the experiments performed by Ahmed *et al.* [9] for the original BCFCM method is that we assume 4 classes for simulated and real brain images (Bg, WM, GM, and CSF) while Ahmed *et al.* assumed 3 classes only (Bg, WM, and GM) by merging the CSF tissue with the background (Bg). Moreover, the

experiments performed by Yuan *et al.* [10] for the BCFCM_WA method focused on segmenting the white matter (WM) tissue only, which is a simpler task than considering all tissues together. This may justify why these methods have issues in our experiments while they succeed in their experiments. Our settings are more challenging and more realistic in terms of the underlying medical application, and we have been able to show that our improved methods outperform the original algorithms in all cases including synthetic data, simulated MRI brain data, and real MRI brain data.

Our improvements not only outperform the original methods in the accuracy of the segmentation results but also in the number of iterations required to get this accuracy. Figure 10 shows the number of iterations for different log bases and different choices of parameter n (in addition to the respective segmentation accuracies). Table 5 also lists the required number of iterations for the examples given above. Obviously, our improved versions need significantly less iterations and the complexity within an iteration is also reduced as the bias field estimation is only carried out once every n-th iterations.

To investigate how much our solution increases the performance of segmentation algorithm in term of computation time and segmentation accuracy for different parameter settings, we do experiments on the simulated brain T1-weighted MR image corrupted with 7% Gaussian noise and 20% intensity inhomogeneity, see Figure 10. In this experiment, we measure the segmentation accuracy and the number of iterations required for the two improved methods using different log bases (1.12, 1.15, 1.18, 1.2, 1.4, 1.44, 1.5, 1.8, 2, 2.719, 3, 5, and 10) and different choices of n (2, 3, 4, and 5).

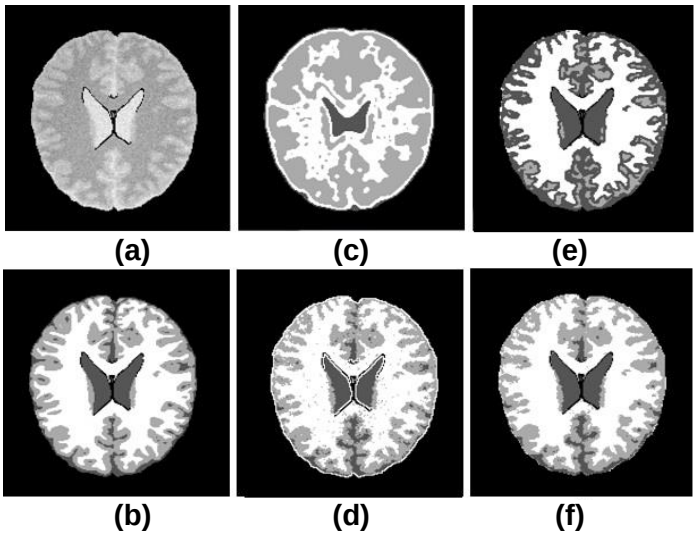

Figure 7: Comparison of segmentation results on simulated PD-weighted MR brain image corrupted with 5% Gaussian noise and 20% intensity inhomogeneity: (a) original image corrupted with noise, (b) ground truth segmentation, (c) BCFCM result, (d) IBCFCM result, (e) BCFCM_WA result, (f) IBCFCM_WA result.

Table 3: Segmentation accuracy (SA) in percentage for the four methods on simulated T1- and T2-weighted MR brain image corrupted with different combinations of noise.

Noise Type	MRI	BCFCM	IBCFCM	BCFCM_WA	IBCFCM_WA
Gaussian 3%	T1	83.4127	97.7264	91.8324	98.699
Gaussian 5%	T1	84.5609	97.2503	91.3028	98.1287
Gaussian 7%	T1	84.4158	96.5221	91.5039	97.8079
IIh*20% & G3%	T1	85.7347	97.1714	91.6185	0.98.2178
IIh 20% & G5%	T1	84.9377	96.8251	91.2799	97.8664
IIh 20% & G7%	T1	85.34	96.7207	91.7967	97.5431
Gaussian 3%	T2	77.2208	96.1428	92.3263	97.7875
Gaussian 5%	T2	80.6146	95.3841	92.0335	96.5272
Gaussian 7%	T2	81.4293	93.7266	92.031	94.0296
IIh*20% & G3%	T2	77.3583	96.25231	91.8451	97.9479
IIh 20% & G5%	T2	79.0921	94.6508	91.7636	96.0435
IIh 20% & G7%	T2	78.784	93.6782	92.5071	93.9227

* IIh=Intensity Inhomogeneity; G=Gaussian

Table 4: Segmentation accuracy (SA) in percentage for the four methods on simulated PD-weighted MR brain image corrupted with different combinations of noise.

Noise Type	BCFCM	IBCFCM	BCFCM_WA	IBCFCM_WA
Gaussian 3%	79.1506	95.0073	77.1418	96.6851
Gaussian 5%	81.9258	93.8615	90.3888	95.8016
Gaussian 7%	79.749	91.4607	85.9256	94.2384
Gaussian 9%	74.5882	87.9573	80.9634	92.3161
IIh*20% & G3%	82.1422	93.9685	89.4111	95.0887
IIh 20% & G5%	81.4192	92.7795	84.9505	94.1925
IIh 20% & G7%	83.0257	89.7497	86.5417	92.9272

* IIh=Intensity Inhomogeneity; G=Gaussian

The experiment shows that, in general, the accuracy increases when the log base decreases, which confirms our theoretical investigations. Also, the accuracy increases when n increases, which, again, confirms our theoretical investigations. The experiment also shows that the number of iterations required to achieve this accuracy decrease as n increases and slightly increases as the log base decreases. Moreover, the result shows that the improved methods outperform the original methods in all cases (*i.e.*, for all tested combinations of log base and n) in terms of number of iterations and segmentation accuracy.

Another observation is that the impact of parameter n is larger than the impact of choosing the log base for improving the results. Hence, we can conclude that the biggest error source in the original BCFCM methods is that the bias field estimation is inaccurate as long as the cluster representatives have not reached a suitable value yet. The inaccurate values of cluster representatives in early iterations lead to inaccurate bias field estimation because of error accumulations which in turn leads to inaccurate cluster representatives estimation for the next iterations, and so on. Our modification gives enough time for the cluster representatives to be configured well before starting the next bias field estimation update.

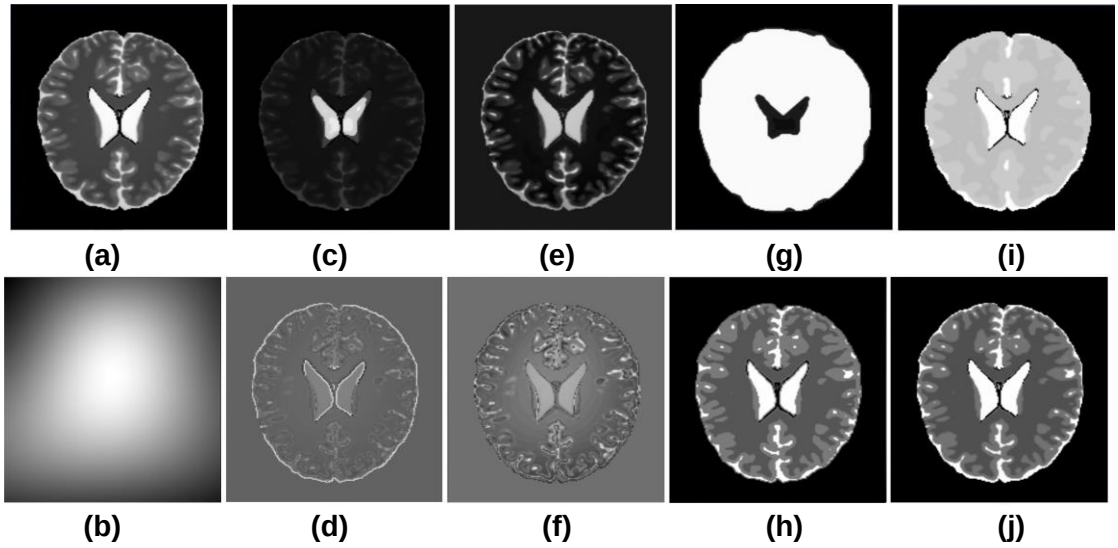

Figure 8: Comparison of bias field estimation and the corrected image on simulated T2-weighted MR image corrupted with 40% intensity inhomogeneity, (a) original image corrupted with 40% intensity inhomogeneity, (b) original bias field , (c) BCFCM bias field, (d) IBCFCM bias field, (e) BCFCM_WA bias field, and (f) IBCFCM_WA bias field, (g) BCFCM corrected image, (h) IBCFCM corrected image, (i) BCFCM_WA corrected image, and (j) IBCFCM_WA corrected image.

Table 5: Segmentation accuracy (SA) in percentage and the number of iterations when applying the four methods and the standard FCM on real brain images of Figure 9.

Fig. 9 (a)	FCM	BCFCM	IBCFCM	BCFCM_WA	IBCFCM_WA
SA*	92.9108	93.6813	96.3333	96.6614	97.3526
NoIt*.	29	120	5	40	4
Fig. 9 (h)	FCM	BCFCM	IBCFCM	BCFCM_WA	IBCFCM_WA
SA	93.0695	93.6813	96.6171	96.6049	97.8088
NoIt.	34	120	6	45	4

* SA=Segmentation accuracy; NoIt.=No. of iterations

The results show that only one or two update of the bias field estimation are required for the convergence criteria to be met achieving better results with a lower number of iterations. One more observation drawn from the results that the IBCFCM_WA method in the contrary to the BCFCM_WA method does not affected very much by the alpha parameter (see Figure 10). We performed similar experiments on the real brain T1-weighted MRI images shown in Figure 9 and we got similar results. From the two experiments with simulated and real brain data, we conclude that the optimal choice of the parameters that gives us the best tradeoff between the segmentation accuracy and the number of iterations is using n=5 with log base 1.44. In general, when fixing n to 5, we can improve the segmentation accuracy by decreasing the log base from 2.71 till 1.2 or we can improve the computation time by increasing the log base at the expense of reducing segmentation accuracy. Since the computational complexity of the approaches by Wang *et al.* [13] and Ji *et al.* [14] is very high when compared to the

FCM and its variants (because of D_{ik} computation), we could not perform a comparison with those approaches and only compare our proposed algorithms to the CLIC algorithm. To compare our methods with the CLIC algorithm [12], we applied the CLIC algorithm on the synthetic image corrupted with mixed noise, the simulated T1-, T2-, and PD-weighted MR images corrupted with 5% Gaussian noise and 20% intensity inhomogeneity, and real MR images. We can observe from the visual and numerical comparison results shown in Figure 11 and Table 6 that our algorithms outperforms CLIC algorithm in both the segmentation accuracy and the number of iterations. If the termination criterion is not met after 120 iterations, we forced the CLIC algorithm to stop.

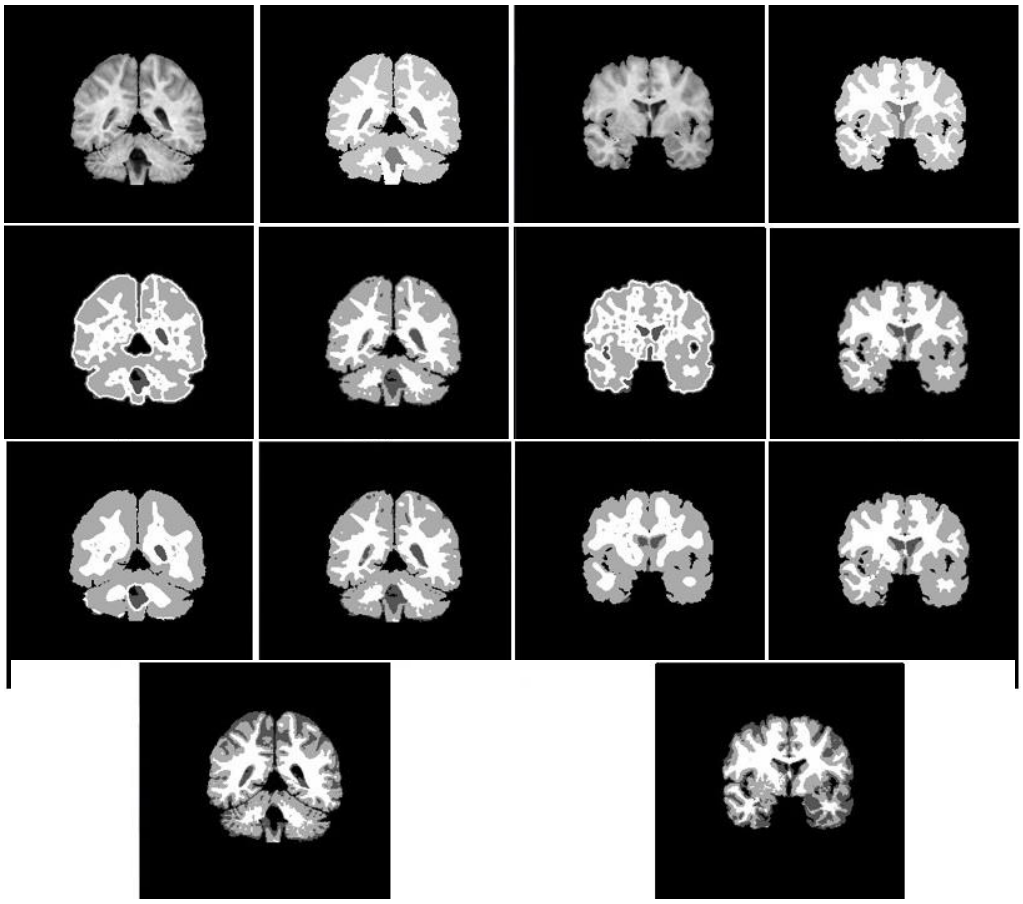

Figure 9: Comparison of segmentation results on real MRI T1-weighted brain image from 17 database: (a) original image (slice no. 12_3_21), (b) its ground truth, (c) BCFCM result, (d) IBCFCM result, (e) BCFCM_WA result, (f) IBCFCM_ WA result, (g) standard FCM result, (h) original image (slice no. 12_3_34), (i) its ground truth, (j) BCFCM result, (k) IBCFCM result, (l) BCFCM_WA result, (m) IBCFCM_WA result, (n) standard FCM result.

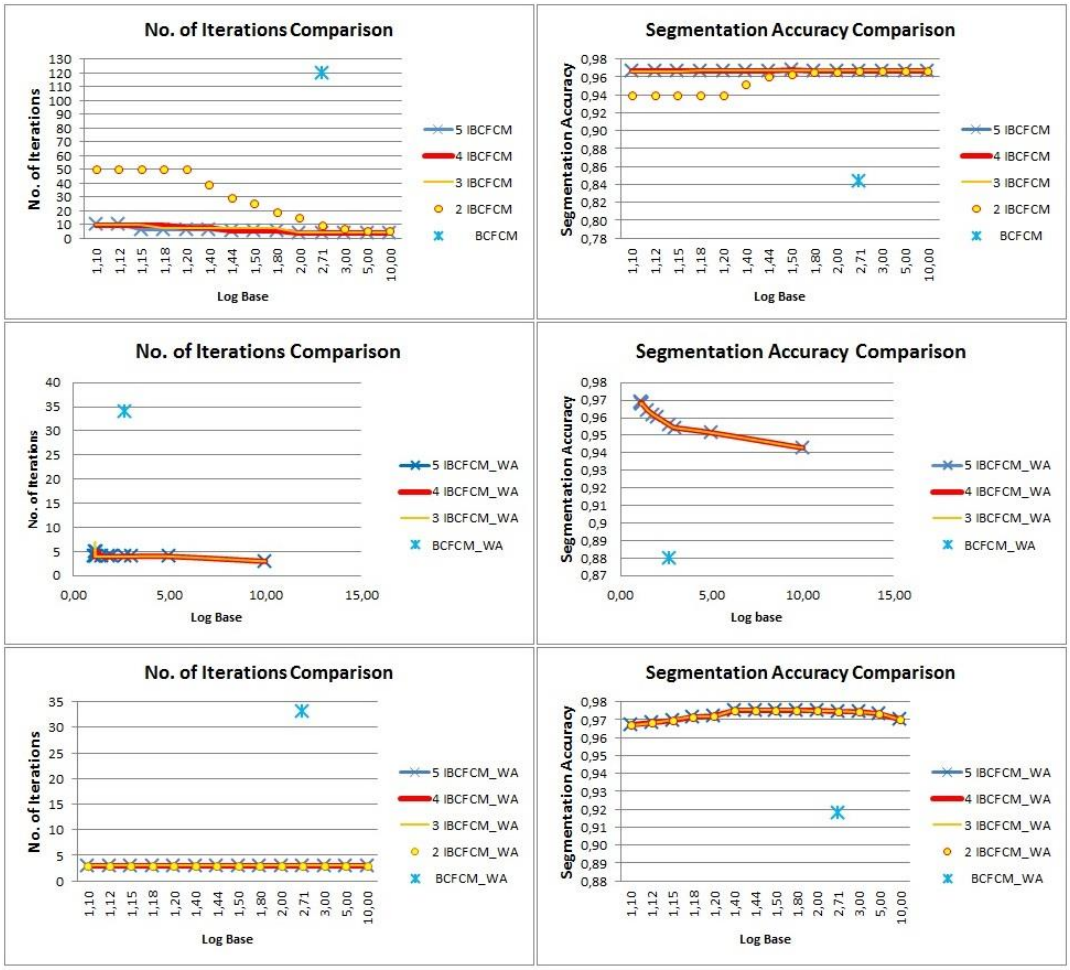

Figure 10: Comparison of number of iterations and segmentation accuracy: (upper) Comparison of IBCFCM for different combinations of n and log base parameters and BCFCM; (middle) comparison of IBCFCM_WA for different combinations of n and log base parameters and BCFCM_WA (using α=1), (lower) comparison of IBCFCM_WA for different combinations of n and log base parameters and BCFCM_WA (using α=0.09).

Table 6: Comparison of segmentation accuracy (SA) in percentage and number of iterations for IBCFCM and IBCFCM_WA with CLIC method on the above images.

Method	CLIC	IBCFCM	IBCFCM_WA	CLIC	IBCFCM	IBCFCM_WA
Measure	SA%*	SA%	SA%	NoIt.*	NoIt.	NoIt.
Fig. 3(a)	88,8061	95.5399	98.8068	120	4	3
Fig. 5(a)	94,1390	96.8251	97.8664	120	6	3
Fig. 6(a)	88,5556	94.6508	96.0435	120	4	3
Fig. 7(a)	84.3598	92.7795	94.1925	120	4	3
Fig. 9(a)	95.7031	96.3333	97.3526	120	5	4
Fig. 9(h)	96.5271	96.6171	97.8088	120	6	4

* SA=Segmentation accuracy; NoIt.=No. of iterations

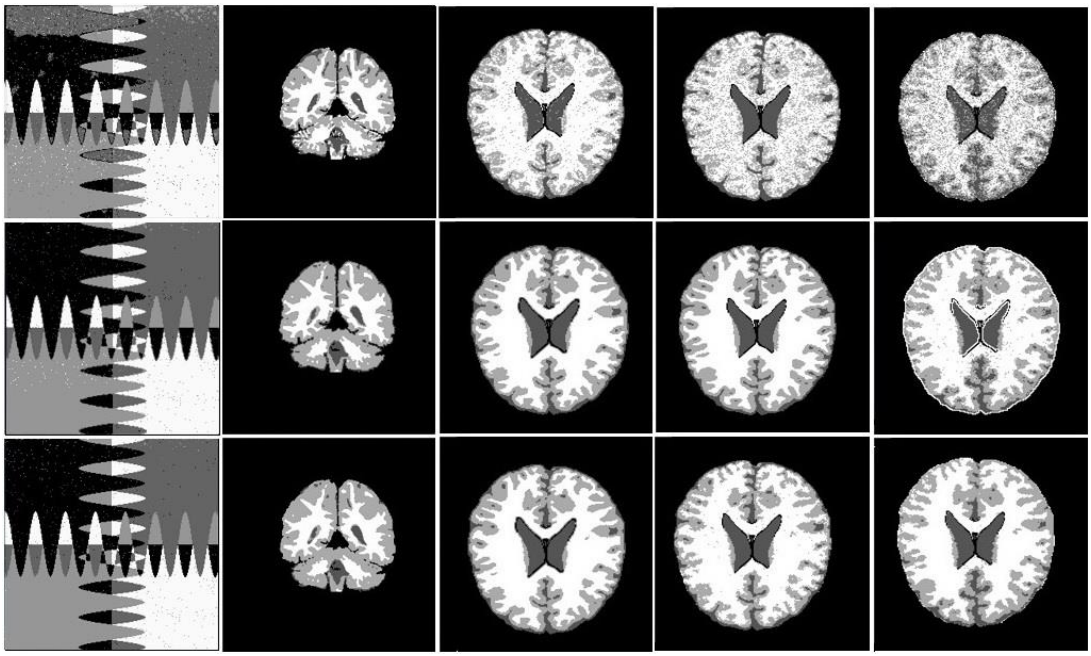

Figure 11: Comparison of IBCFCM and IBCFCM_WA with CLIC method using the synthetic image with mixed noise, real MRI, and the simulated (T1-, T2-, and PD-weighted) MRI: the segmentation result of CLIC (first row), IBCFCM (2nd row), and IBCFCM_WA (3rd row).

In addition to the sensitivity of the CLIC algorithm to the choice of the parameter of the weighting function, the CLIC algorithm omits the local gray level relationship in its criterion function. This may lead to inaccurate estimation of the membership functions, and finally cause misclassifications, especially for the pixels around the boundaries and for MR images that have tissues with very similar intensities such as T2- and PD-weighted MR images.

6. Conclusions

Image segmentation plays an important role in analyzing medical images for different applications such as surgical planning, radiotherapy treatment, or pathology detection. The presence of different kinds of artifacts in medical image processing pipeline leads to uncertain segmentation results, which may cause wrong decisions like performing unnecessary surgery or giving inaccurate radiotherapy dose. In this paper, we improve the result of BCFCM segmentation algorithms by reducing the effect of some uncertainty sources on these results. Our improvement gives enough time for the estimated clusters to be configured well before the bias field estimation is updated. The implementation of the improved and the original methods on synthetic, simulated (T1-, T2-, and PD-weighted) brain MR images, and real T1-weighted MR images show that our improved methods outperform the original methods in term of both the segmentation accuracy and the number of iterations which means that the aggregated uncertainty is reduced consequently. In our experiments, three to six iterations were enough to get segmentation accuracies that clearly outperforms the original method.

References

[1] C. Guttmann, F. A. Jolesz, R. Kikinis, R. Killiany, M. Moss, T. Sandor, and M. Albert, "White matter changes with normal aging", Neurology, vol. 50, no. (**1998)**, pp. 972-978.
[2] W. C. Heindel, T. L. Jernigan, S. L. Archibald, C. L. Achim, E. Masliah, and C. A. Wiley, "The relationship of quantitative brain magnetic resonance imaging measures to neuropathologic indexes of human immunodeficiency virus infection", Archives of Neurology, vol. 51, (**1994**), pp. 112-935.
[3] N. A. Mohamed, M. N. Ahmed, and A. Farag, "Modified fuzzy c-mean in medical image segmentation". In Proceedings IEEE International Conference on Acoustics, Speech, and Signal Processing, 1999, Piscataway, NI USA, volume 6, pages 3429-3432 vol. 6, (**1999**).
[4] D. L. Pham., "Fuzzy clustering with spatial constraints", In International Conference on Image Processing, 2002 Proceedings, volume 2, pages II-65-II-68 vol.2, (**2002**).
[5] S. Chen and D. Zhang, "Robust image segmentation using FCM with spatial constraints based on new kernel-induced distance metric", IEEE Trans. on System, Man. and Cybernetics-Part B, 34(4):1907-1916, (**2004**).
[6] D. Zhang and S. Chen, "A novel kernelised fuzzy c-means algorithm with application in medical image segmentation", Artificial Intelligence in Medicine, 32(1):37-50, (**2004**).
[7] K.-S. Chuang, H.-L. Tzeng, S. Chen, J. Wu, and T.-J. Chen, "Fuzzy c-means clustering with spatial information for image segmentation", Computerized Medical Imaging and Graphics, 30(1): 9-15, (**2006**).
[8] W. Cai, S. Chen, and D. Zhang, "Fast and robust fuzzy c-means clustering algorithms incorporating local information for image segmentation", Pattern Recognition, 40(3):825-838, (**2007**).
[9] M. N. Ahmed, S. M. Yamany, N. Mohamed, A. A. Farag, and T. Moriarty, "A modified fuzzy c-means algorithm for bias field estimation and segmentation of MRI data", IEEE Transactions on Medical Imaging, 21(3):193-199, March (**2002**).
[10] K. Yuan, L. Wu, Q. S. Cheng, S. Bao, C. Chen, and H. Zhang, "A novel fuzzy c-means algorithm and its application", International Journal of Pattern Recognition and Artificial Intelligence, 19(8):1059-1066, (**2005**).
[11] L. Szilágyi, Z. Benyo, S. M. Szilágyi, and H. S. Adam, "MR brain image segmentation using an enhanced fuzzy c-means algorithm", In Proceedings of the 25th Annual International Conference of the IEEE, volume 1, pages 724-726. Engineering in Medicine and Biology Society, 17-21 Sept. (**2003**).
[12] C. Li, C. Xu, A.W. Anderson, and J.C. Gore. "MRI tissue classification and bias field estimation based on coherent local intensity clustering: A unified energy minimization framework", in Information Processing in Medical Imaging: Proceedings of the 21st International Conference, IPMI 2009,Williamsburg, VA, USA, July 5–10, 2009, vol. 5636 of Lecture Notes in Computer Science, pp. 288–299, Springer, Berlin, Germany, (**2009**).
[13] J. Wang, J. Kong, Y. Lu, M. Qi, and B. Zhang, "A modified FCM algorithm for MRI brain image segmentation using both local and non-local spatial constraints", Computerized Medical Imaging and Graphics, 32(8):685- 698, (**2008**).
[14] Z.-X. Ji, Q.-S. Sun, and D.-S. Xia, "A modified possibilistic fuzzy c-means clustering algorithm for bias field estimation and segmentation of brain MR image", Computerized Med. Imag. and Graphics, 35(5):383- 397, (**2011**).
[15] J.C. Bezdek, "Pattern recognition with fuzzy objective function algorithms", Plenum, NY. (**1981**).
[16] MNI, "Brainweb: simulated brain database", Access time: on November 2012; Available at: http://www.bic.mni.mcgill.ca/brainweb/., (**1997**).
[17] IBSR, "The internet brain segmentation repository", Access time: on October 2012; Available at: http://www.cma.mgh.harvard.edu/ibsr/., (**1996**).

Authors

Ahmed A Abdulredha Al-Taie, he received his B.S. degree in 1997 and M.Sc. degree in 2000 in Computer Science both were from Department of Computer Science, University of Baghdad, Baghdad, Iraq. He joined the Department of Computer Science of College of Science for Women at the University of Baghdad, Iraq, as an assistant teacher in 2005. Currently, he is working on his Ph.D. in the Visualization and Computer Graphics Laboratory (VGCL) at the School of Engineering and Science in Jacobs University, Bremen, Germany. His research interests include Medical Image Analysis and Processing.

Horst K. Hahn, he studied physics with mathematics, computer science, and physiology as minors at the University of Bayreuth, Universitée Paul Sabatier Toulouse III, and Ruprecht-Karl University Heidelberg. He authored six patents and more than 175 refereed scientific journal and conference publications in the fields of computer-assisted medicine, quantitative medical imaging, computer-aided detection and diagnosis of cancer, neuroimaging, and image-guided therapy. In 2006, he became vice president of the non-profit MeVis Research GmbH and was centrally involved in its transformation into the Fraunhofer Institute for Medical Image Computing MEVIS as of January 2009, where he acts as institute director since Oct 2012. At the age of 35, he became adjunct professor of medical visualization and four years later professor of medical imaging at Jacobs University Bremen. He is scientific coordinator of several national and European research consortia, and, among other prices and awards, received the Bremer Studienpreis - Special Price Bruker Daltonik for his PhD thesis entitled "Morphological Volumetry – Theory, Concepts, and Application to Quantitative Medical Imaging". Not least, he organized in July 2011 the prestigious International Conference on Information Processing in Medical Imaging together with Gabor Szekely, ETH Zurich, for the first time in Germany.

Lars Linsen, he is a Full Professor of Computational Science and Computer Science at the School of Engineering and Science of the Jacobs University, Bremen, Germany. He received his academic degrees from the Universität Karlsruhe (TH), Germany, including a diploma in computer science in 1997 and a Ph.D. in computer science in 2001. He spent three years as a post-doctoral researcher and lecturer at the Institute for Data Analysis and Visualization (IDAV) and the Department of Computer Science of the University of California, Davis, U.S.A. He joined the Department of Mathematics and Computer Science of the Ernst-Moritz-Arndt-Universität Greifswald, Germany, as an assistant professor in 2004. In 2006, he joined Jacobs University as an associate professor and became a full professor in 2012. Lars Linsen's research interests are mainly in the areas of (spatial and non-spatial) data visualization and include certain topics in computer graphics and geometric modeling.